Monthly Notices
of the
ROYAL ASTRONOMICAL SOCIETY

Mon. Not. R. Astron. Soc. **423,** 2617–2626 (2012) doi:10.1111/j.1365-2966.2012.21063.x

# A large-scale structure traced by [O II] emitters hosting a distant cluster at $z = 1.62$

Ken-ichi Tadaki,[1⋆] Tadayuki Kodama,[2] Kazuaki Ota,[3] Masao Hayashi,[4] Yusei Koyama,[4] Casey Papovich,[5,6] Mark Brodwin,[7] Masayuki Tanaka[8] and Masanori Iye[1,4]

[1]*Department of Astronomy, Graduate School of Science, University of Tokyo, Tokyo 113-0033, Japan*
[2]*Subaru Telescope, National Astronomical Observatory of Japan, 650 North Afohoku Place, Hilo, HI 96720, USA*
[3]*Department of Astronomy, Kyoto University, Kitashirakawa-Oiwake-cho, Sakyo-ku, Kyoto 606-8502, Japan*
[4]*Optical and Infrared Astronomy Division, National Astronomical Observatory of Japan, Mitaka, Tokyo 181-8588, Japan*
[5]*Department of Physics and Astronomy, Texas A&M University, College Station, TX 77845-4242, USA*
[6]*George P. and Cynthia Woods Mitchell Institute for Fundamental Physics and Astronomy College Station, TX 77843, USA*
[7]*Department of Physics, University of Missouri, 5110 Rockhill Road, Kansas City, MO 64110, USA*
[8]*Institute for the Physics and Mathematics of the Universe, University of Tokyo, Kashiwanoha, Kashiwa, Chiba 277-8582, Japan*

Accepted 2012 April 5. Received 2012 April 4; in original form 2011 October 26

**ABSTRACT**

We present a panoramic narrow-band imaging survey of [O II] emitters in and around the ClG J0218.3−0510 cluster at $z = 1.62$ with Suprime-Cam on Subaru Telescope. 352 [O II] emitters were identified on the basis of narrow-band excesses and photometric redshifts. We discovered a huge filamentary structure with some clumps traced by [O II] emitters and found that the ClG J0218.3−0510 cluster is embedded in an even larger superstructure than the one reported previously. 31 [O II] emitters were spectroscopically confirmed with the detection of H$\alpha$ and/or [O III] emission lines by Fibre Multi Object Spectrograph observations. In the high-density regions such as cluster core and clumps, star-forming [O II] emitters show a high overdensity by a factor of more than 10 compared to the field region. Interestingly, the relative fraction of [O II] emitters in photo-$z$ selected sample does not depend significantly on the local density. Although the star formation activity is very high even in the cluster core, some massive quiescent galaxies also exist at the same time. Furthermore, the properties of the individual [O II] emitters, such as star formation rates (SFRs), stellar masses and specific SFRs, do not show a significant dependence on the local density, either. Such a lack of environmental dependence is consistent with our earlier result by Hayashi et al. on a $z = 1.5$ cluster and its surrounding region. The fact that the star-forming activity of galaxies in the cluster core is as high as that in the field at $z \sim 1.6$ may suggest that the star-forming galaxies are probably just in a transition phase from a starburst mode to a quiescent mode, and are thus showing comparable level of star formation rates to those in lower density environments. We may be witnessing the start of the reversal of the local SFR–density relation due to the 'biased' galaxy formation and evolution in high-density regions at this high redshift, beyond which massive galaxies would be forming vigorously in a more biased way in protocluster cores.

**Key words:** galaxies: clusters: individual: ClG J0218.3−0510 – galaxies: evolution – large-scale structure of Universe.

## 1 INTRODUCTION

It is widely known that the formation and evolution of galaxies strongly depend on their surrounding environments. Galaxy clusters are the most massive object and the densest structures in the Universe. As such, clusters and their surrounding regions serve as ideal sites for studying the roles of galaxy environment on galaxy formation and evolution. In the local Universe, it is known that the star formation has already ceased a long time ago in high-density regions such as clusters and most of the galaxies therein are only passively evolving since then, while galaxies in the general field

⋆E-mail: tadaki.ken@nao.ac.jp

are still actively forming stars even at the present day (e.g. Lewis et al. 2002; Gómez et al. 2003; Kauffmann et al. 2004). Such environmental variation has been well recognized as a sharp correlation between galaxy morphology and local number density of galaxies (e.g. Dressler 1980; Postman & Geller 1984; Whitmore, Gilmore & Jones 1993; Dressler et al. 1997). In clusters at $z \sim 1$, Muzzin et al. (2012) found that the specific star formation rate (SSFR) of star-forming galaxies is independent of environment at a fixed stellar mass, but the fraction of star-forming galaxies is decreased in high-density environment. This suggests that the environmental-quenching time-scale would be rapid. Recent observations are discovering very distant clusters at $z \sim 1.5$–2.0 (Henry et al. 2010; Papovich et al. 2010; Tanaka, Finoguenov & Ueda 2010; Brodwin et al. 2011; Fassbender et al. 2011; Gobat et al. 2011). It is crucial to observe clusters at such frontier redshifts so as to directly witness and understand the early evolution of galaxies and the physical processes which are responsible for the strong environmental dependence of galaxy properties at later times.

To survey star-forming galaxies with a narrow-band filter, which captures nebular emission lines such as H$\alpha$ and [O II], is very efficient and effective for studying cluster galaxies because we can construct a large sample of star-forming galaxies without any expensive spectroscopic observation. The correlation between the star formation activity, traced by a nebular emission, and the environment has already been investigated by many authors rather intensively. For field environment and groups at $z = 0.84$, Sobral et al. (2011) have constructed a large sample of H$\alpha$ emitters with a narrow-band filter as a part of the High-$z$ Emission Line Survey (HiZELS), and found that the fraction of star-forming galaxies falls sharply as a function of local number density of photo-$z$ sample from about 40 per cent in the field to almost zero in rich groups. For clusters at $z \sim 0.5$–1.5, our previous studies on H$\alpha$ emitters in CL0939+4713 (Abell 851) at $z = 0.41$ and in RX J1716.4+6708 at $z = 0.81$ show that the fraction of emitters decreases towards cluster central region, and the star formation activity peaks in the intermediate-density regions such as groups and filaments at the cluster outskirts (Koyama et al. 2011, 2010). On the other hand, the studies in higher redshift clusters ($z \sim 1.5$) have produced two different results. While there are no H$\alpha$ emitters within a radius of 200 kpc from the centre of the most massive cluster XMMU J2235.3−2557 at $z = 1.39$ (Bauer et al. 2011), the other cluster XMMXCS 2215.9−1738 at $z = 1.46$ (Hayashi et al. 2010) shows much higher star formation activity as traced by [O II] emitters even in the cluster core. One possible interpretation would be that in a more massive system galaxy evolution is accelerated and star formation is truncated at an earlier epoch. However, there is a caveat that some of the [O II] emitters in the cluster core may be contaminated by active galactic nucleus (AGN).

To obtain more general picture on the star formation history in clusters, we need to study many clusters at each epoch. In fact, we are currently conducting the MApping HAlpha and Lines of Oxygen with Subaru (MAHALO-Subaru project; Kodama et al., in preparation), which is a large and systematic narrow-band survey of star-forming galaxies in many clusters at $z \sim 1.5$–3.0 and in the field. This paper reports one of the initial results of the project. This survey will provide us with the dependence of star formation history on environment.

We comment here, however, that if we only target clusters that have already formed and matured at each epoch, the results may be biased towards apparently weaker evolution. This difficult problem should be tackled by targeting lower mass systems as well as the rich clusters. By tracing the surrounding large-scale structures around rich clusters, however, we can automatically include many smaller mass groups and/or filaments embedded in the structures. This is another good advantage of panoramic studies of distant clusters like ours.

In this paper, we report a narrow-band survey of [O II] emitters in and around the spectroscopically confirmed distant cluster ClG J0218.3−0510 (IRC 0218-A) at $z = 1.62$ (Papovich et al. 2010; Tanaka et al. 2010) and is in Subaru/*XMM–Newton* Deep Survey Field (SXDS; Furusawa et al. 2008). The coordinates of this cluster are $\alpha = 2^{\rm h}18^{\rm m}21.3^{\rm s}$, $\delta = -5^{\circ}10'27''$ (J2000), derived from the centroid of the sources selected by *Spitzer* Infrared Array Camera (IRAC) colour in this overdensity. We assume cosmological parameters of $H_0 = 70\,{\rm km\,s^{-1}\,Mpc^{-1}}$, $\Omega_{\rm M} = 0.3$ and $\Omega_\Lambda = 0.7$, and adopt AB magnitudes throughout this paper. At $z = 1.62$, 1 arcsec corresponds to 8.47 kpc in a physical distance and to 22.20 kpc in a comoving distance.

## 2 OBSERVATIONS AND DATA

### 2.1 Imaging data

To identify line emitters, we used a narrow-band filter (*NB*973) and a medium-band filter ($z_R$). The *NB*973 filter ($\lambda_{\rm c} = 9755$ Å, $\Delta\lambda_{\rm FWHM} = 202$ Å) can detect an [O II] line emission at $1.590 \leq z \leq 1.644$ and $z_R$ filter ($\lambda_{\rm c} = 9860$ Å, $\Delta\lambda_{\rm FWHM} = 590$ Å) can measure a continuum flux at the same wavelength range as the *NB*973 filter. These filters enable us to sample most of the star-forming galaxies associated with the cluster at $z = 1.62$ as shown in Fig. 1. The imaging data with *NB*973 filter were obtained in an area between the SXDS-C and SXDS-S by Ota et al. (2010). The seeing size in the combined image is 1.0 arcsec and the $5\sigma$ limiting magnitude is 25.4 in a 2.0-arcsec diameter aperture. The details of the observations and the data reduction are described in Ota et al. (2010). For the $z_R$ data, we conducted a new observation with Subaru Prime Focus Camera (Suprime-Cam; Miyazaki et al. 2002) on the Subaru Telescope in October 2010. The weather was good during our observation, and the sky conditions were photometric with the

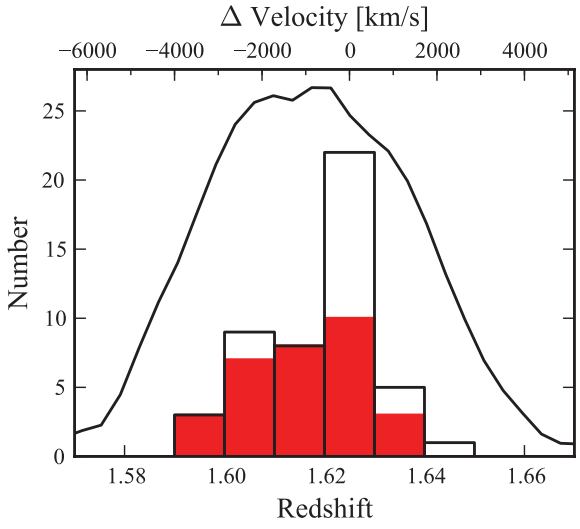


**Figure 1.** A transmission curve (solid line) of *NB*973 filter and the redshift distribution (black histogram) of spectroscopically confirmed galaxies, including the cluster members in the literatures (Papovich et al. 2010; Tanaka et al. 2010). The [O II] emitters whose redshifts are derived from our FMOS observation are shown by red histogram.

seeing of 0.5–0.7 arcsec. Data reduction was carried out in a normal manner with SDFRED (Yagi et al. 2002; Ouchi et al. 2004). The frames for the total of 327 min are integrated in the final image. The field coverage is 830 arcmin$^2$, corresponds to $1.4 \times 10^5$ Mpc$^3$ in the survey volume. The $5\sigma$ limiting magnitude is 25.3 in a 2.0-arcsec diameter aperture. Point spread function (PSF) of the $z_R$ image was degraded to 1.0 arcsec to match the quality of the *NB*973 image.

### 2.2 Photometric catalogue

In the SXDS field, many multiwavelength data are already available. In this work, we used a total of 12 multiband data including the *NB*973 and $z_R$-band ones. Deep optical broad-band images ($B$, $V$, $R$, $i'$, $z'$) were taken by the Suprime-Cam (Furusawa et al. 2008). For near-infrared wavelength, the UKIDSS Ultra Deep Survey (UKIDSS-UDS; Lawrence et al. 2007) has been conducted in this region, and we used the Data Release 8 (DR8) data ($J$, $H$, $K$). The photometric system and calibration are described by Hewett et al. (2006) and Hodgkin et al. (2009), respectively. From 10-band (*NB*973, $B$, $V$, $R$, $i'$, $z'$, $z_R$, $J$, $H$, $K$) images, we made a photometric catalogue using SExtractor (Bertin & Arnouts 1996). PSFs of all the images were matched to 1.0 arcsec and the positions were matched with respect to the *NB*973 image. A source detection was performed on the *NB*973 image. The extraction criteria were at least nine pixels with fluxes above $2\sigma$ level, where $1\sigma$ is the sky noise of the image. The sources fainter than $5\sigma$ limiting magnitude in *NB*973 were rejected. Photometries in all the images were carried out using the double image mode. An aperture magnitude within a diameter of 2 arcsec was used to derive a colour, and Kron magnitude was used to calculate a total magnitude (Kron 1980). For mid-infrared wavelength, we used IRAC catalogue (only 3.6 and 4.5 μm) for a *Spitzer* Public Legacy Survey of the UKIDSS-UDS (SpUDS; PI: J. Dunlop). From our catalogue, we identified sources that have an association in the IRAC catalogue within a 1.0-arcsec radius. Moreover, not only the *NB*973-detected catalogue, but also the $K$-detected one was created above $5\sigma$ in the same manner when we select passively evolving galaxies later in Section 3.3. The *NB*973-detected and the $K$-detected catalogues include 39 229 and 40 786 objects respectively, of which 33 242 objects are in common.

### 2.3 Spectroscopy

Near-infrared spectroscopy of our photometrically identified [O II] emitter candidates was conducted with Fibre Multi Object Spectrograph (FMOS; Kimura M. et al. 2010) on the Subaru Telescope in 2012 January. Observations were made with low-resolution (LR) mode in IRS1 and high-resolution (HR) mode at $J$-long and $H$-long bands in IRS2. LR, $J$-long and $H$-long modes can cover the wavelength ranges 1.0–1.8, 1.12–1.35 and 1.59–1.80 μm, respectively. Cross-beam switching mode was adopted and the total integration times were 375 min in LR, 60 min in $J$-long and 300 min in $H$-long mode. The seeing was typically 1 arcsec in $R$ band during observations. Reduction was carried out with the FMOS pipeline FIBRE-PAC (Iwamuro et al. 2012). The flux calibration was done using some F-, G- or K-type stars from the Two Micron All Sky Survey (2MASS; Skrutskie et al. 2006), observed simultaneously. The flux loss was estimated to roughly 50 per cent for a point source and this might be caused by various factors (e.g. weather condition, instrument focus and position error in the catalogue). In this paper, only spectroscopic redshifts, derived from fitting emission lines, are used in order to estimate the accuracy of the photometric redshift and the level of completeness and contamination. Other analyses such as line fluxes, line widths and line ratios will be presented in detail in our forthcoming paper. Also, we used the catalogues of spectroscopic redshifts from Simpson et al. (2012) and Smail et al. (2008).

## 3 TARGET SELECTION

In order to investigate galaxy evolution, we need to sample both actively star-forming galaxies and passively evolving galaxies at the same epoch. As noted in Section 1, the former can be selected by the presence of nebular emission lines such as [O II]. The latter population can be selected by utilizing the photometric redshift and the colour–colour diagram. Using the multiband data in Section 2, a total of 352 [O II] emitters at $z \simeq 1.62$ have been identified over a 830 arcmin$^2$ area. Also, we have constructed a photo-$z$ selected sample with $M_{\rm star} > 10^{10}$ M$_\odot$ at $1.56 \leq z_{\rm phot} \leq 1.68$, which includes 132 [O II] emitters and 259 quiescent galaxies at $z \simeq 1.6$.

### 3.1 [O II] emitters

We can identify emission line galaxies on the basis of the excesses of *NB*973 fluxes over $z_R$ fluxes. *NB*973-detected catalogue created in Section 2.2 is used. Fig. 2 shows the $z_R - NB973$ colour–magnitude diagram for all the objects satisfying $NB973 > 5\sigma$. Note that we made a correction of $+0.11$ in the $z_R - NB973$ colour because the effective wavelengths of two filters are not exactly the same. For faint objects ($<2\sigma$) in $z_R$ band, $2\sigma$ value was used to calculate colour. If a strong emission line comes into the $z_R$ band but not on the *NB*973 filter (e.g. at $z = 1.58$ or $z = 1.66$), such object may be detected as false absorbers. Also, because the effective wavelength of *NB*973 filter is slightly shorter than that of the $z_R$ filter, very red objects may have negative colours in $z_R - NB973$. Bunker et al. (1995) have defined the significance of the excess in the narrow band by the parameter Σ, with taking into account of the fact that

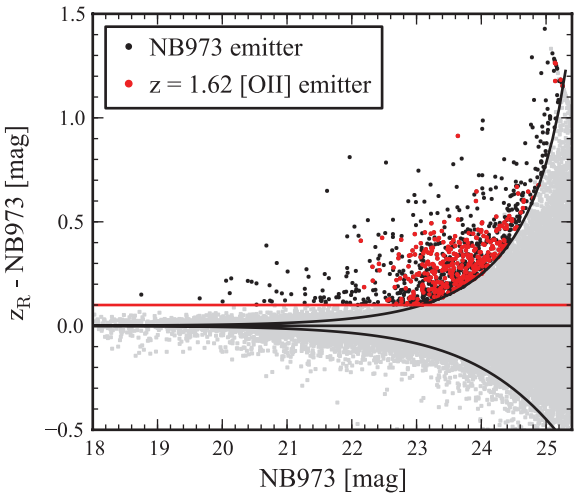


**Figure 2.** $z_R - NB973$ colour–magnitude diagram to select [O II] emitter candidates at $z = 1.62$. Grey dots show all objects with $NB973 > 5\sigma$. Black and red filled circles are *NB*973 emitters and [O II] emitters which satisfy the criteria in Section 3.1.

the fainter the narrow-band flux is, the larger the photometric error is. $\Sigma = 2.5$ was adopted as our first criterion to select narrow band (NB) emitters (Sobral et al. 2009). Since the standard deviation of $z_R - NB973$ is 0.03 in the range $18 < NB973 < 21$, the colour excess of $z_R - NB973 > 0.1$, i.e. corresponds to $3\sigma$ for the bright objects, was also adopted. These criteria correspond to the limiting line flux of $1.8 \times 10^{-17}$ erg s$^{-1}$ cm$^{-2}$, i.e. 4–5 M$_\odot$ yr$^{-1}$ in dust-uncorrected star formation rate (SFR) using the calibration of Kennicutt (1998), and to the equivalent width of about 30 Å in the observed frame. Based on the first criterion, 969 objects are identified as *NB*973 emitters.

The *NB*973 filter can pick out not only [O II] lines at $z = 1.62$ but also some other lines at different redshifts: Ly$\alpha$ at $z = 7.02$, H$\beta$ at $z = 1.01$, [O III] at $z = 0.95$ and H$\alpha$ line at $z = 0.49$. To discriminate between [O II] emitters and those other line emitters, we utilize photometric redshifts for those objects that have satisfied our criteria. Photometric redshifts were determined with the EAZY code (Brammer, van Dokkum & Coppi 2008). 11 band data ($B$, $V$, $R$, $i'$, $z'$, $z_R$, $J$, $H$, $K$, 3.6, 4.5 μm) are used for spectral energy distribution (SED) fitting. Capturing Balmer/4000-Å break, $z_R$ band should improve the accuracy of photometric redshift for galaxies at $z \sim 1.4$–2.0. Because $z_R$ band can be substantially affected by the presence of our target emission line itself, the emission line flux and the emission line subtracted continuum flux density are estimated from the $z_R$- and *NB*973-band fluxes as follows:

$$F_{\rm line} = \Delta_{NB973} \frac{f_{NB973} - f_{z_R}}{1 - \Delta_{NB973}/\Delta_{z_R}}, \quad (1)$$

$$f_{\rm continuum} = \frac{f_{z_R} - f_{NB973}(\Delta_{NB973}/\Delta_{z_R})}{1 - \Delta_{NB973}/\Delta_{z_R}}, \quad (2)$$

where $F_{\rm line}$ is the emission line flux, $f$ denotes a flux density and $\Delta$ indicates a full width at half-maximum (FWHM) of a filter. The emission-line-subtracted flux density in $z_R$ band is used for SED fitting. Fig. 3 is the distribution of the photometric redshift for *NB*973 emitters. We can clearly recognize three peaks in the photometric redshift distribution (i.e. $z \sim 0.5$, 1 and 1.6). These redshift peaks neatly correspond to H$\alpha$, [O III] or H$\beta$, and [O II] respectively, assuring the detection of line emitters as expected.

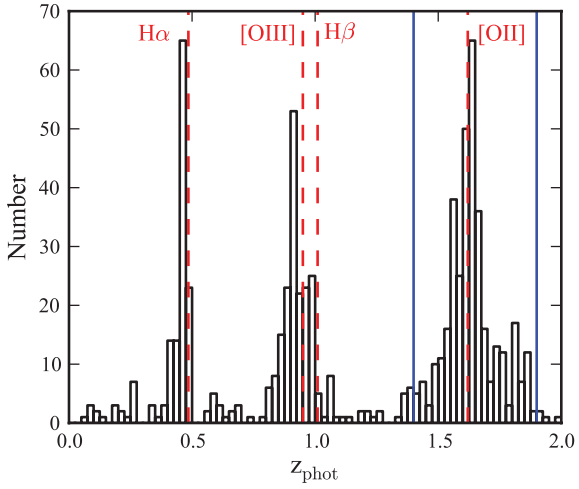


**Figure 3.** The distribution of photometric redshift for *NB*973 emitters. Red dash lines indicate the expected redshift of emission lines that can fall on to the *NB*973 filter (H$\alpha$ at $z \sim 0.49$, [O III] at $z \sim 0.95$, H$\beta$ at $z \sim 1.01$ and [O II] at $z \sim 1.62$). Blue lines indicate the photometric redshift ranges ($1.4 < z_{\rm phot} < 1.9$) to define [O II] emitters.

This also indicates that our first criterion of $\Sigma = 2.5$ and $z_R - NB973 > 0.1$ is effective in identifying secure line emitters. Out of *NB*973 emitters, we down selected 352 [O II] emitters that fall in the range $1.4 < z_{\rm phot} < 1.9$, as second criterion, to distinguish between our target [O II] emitters at $z = 1.62$ and other unwanted line emitters at other redshifts.

While most of the [O II] emitters are likely to be star-forming galaxies, there is a possibility that some of the [O II] emission lines are originated from central AGNs rather than star-forming regions. In particular, some authors reported that 'red' [O II] emitters tend to be contaminated by AGN activities (Yan et al. 2006; Lemaux et al. 2010; Hayashi et al. 2011; Tanaka M. et al. 2012). Alternatively, red emitters are dusty starburst galaxies which are reddened by a large amount of dust extinction. In any case, these red emitters are interesting objects which may be key populations to understanding galaxy evolution in dense environment. However, we cannot disentangle these two possibilities at this stage without spectroscopy. With spectroscopy, we should be able to distinguish between AGNs and dusty starbursts by measuring emission line ratios of [O III]/H$\beta$ and [N II]/H$\alpha$ and plot them on the BPT diagram (Baldwin, Phillips & Terlevich 1981; Kauffmann et al. 2003). Here, we defined red emitters with the $z - J$ versus $J - K$ colour–colour diagram (hereafter $zJK$ diagram) and treated only the [O II] emitters that are outside the quiescent zone defined in Section 3.3 as star-forming galaxies. Also, our criteria of [O II] emitters select three X-ray-detected objects (Ueda et al. 2008), of which two are located at different redshifts. Therefore, the remaining one is not used in our analysis due to some uncertainty. Eventually, we have identified a total of 340 star-forming [O II] emitters and 12 red emitters associated with the cluster at $z = 1.62$.

### 3.2 Spectroscopic follow-up for [O II] emitters

At $z = 1.62$, [O III] and H$\alpha$ emission lines shift to 1.31 and 1.72 μm, respectively. From the *NB*973 emitter sample with $F([{\rm O\,II}]) > 3.0 \times 10^{-17}$ erg s$^{-1}$ cm$^{-2}$ identified in the previous section, 46 (IRS1, LR mode) and 39 objects (IRS2, HR mode) were observed with FMOS. H$\alpha$ emission lines are detected for four objects in LR mode and for 24 objects in $H$-long. [O III] emission lines are detected for seven objects in LR mode and for four objects in $J$-long. The sensitivity of the LR mode is not good enough to detect emission lines due to the large flux loss. If only the $H$-long mode is considered, the detection rate of emission lines is about 60 per cent in total and 80 per cent for bright [O II] emitters with $F([{\rm O\,II}]) > 7.0 \times 10^{-17}$ erg s$^{-1}$ cm$^{-2}$. These values are really good since 20–25 per cent of the wavelength coverage is masked in the FMOS spectrograph due to OH-airglow lines. Fig. 4 shows some examples of H$\alpha$ spectra of our [O II] emitters. Spectroscopic redshifts are derived by Gaussian fitting with free parameters of redshift, line width, and flux densities of H$\alpha$ and [N II]λ6584 or [O III]λ4959, λ5007. As a result, 31 spectroscopic redshifts are obtained in total from the FMOS data, since there are eight objects whose H$\alpha$ and [O III] lines are both detected. There are a total of 42 spectroscopically confirmed galaxies with emission lines, including 11 spectroscopic redshifts with an emission line in the literatures. 40 out of them were selected by the criteria in the previous section. On the other hand, there were no objects with a different redshift in our [O II] emitter sample.

### 3.3 Quiescent galaxies

We also need to select passively evolving galaxies located at $z = 1.62$ to quantify the averaged star formation activity.

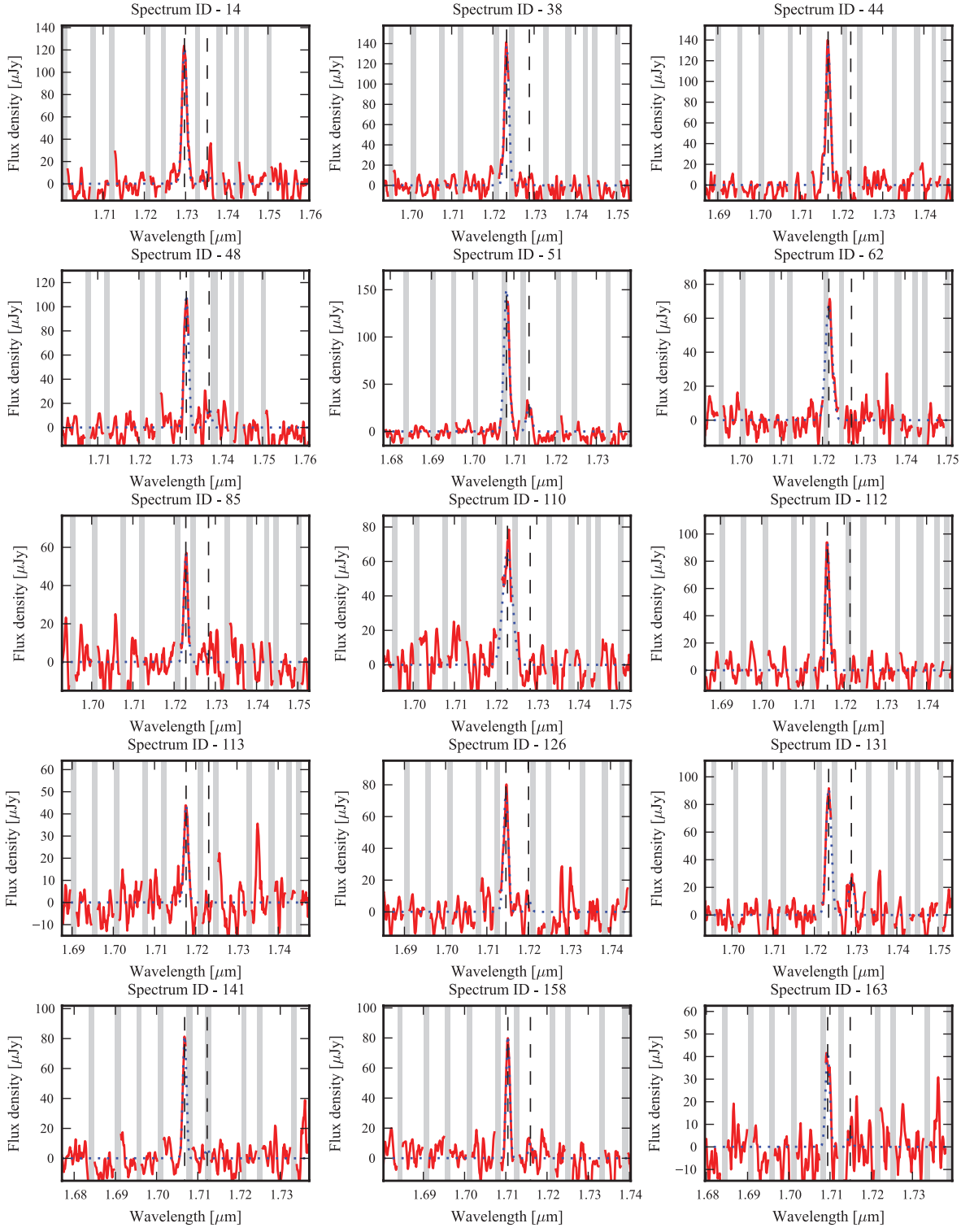


**Figure 4.** Examples of H$\alpha$ spectra for [O II] emitters. Red line and blue dotted line show a observed spectra and a Gaussian fitting spectra, respectively. Vertical dashed lines indicate the redshifted wavelength of H$\alpha$ and [N II]$\lambda$6584. Grey zones indicate the positions of the OH-mask.

First, photometric redshifts were measured for all the objects in the $K$-band-detected catalogue created in Section 2. X-ray-detected objects were rejected because the accuracy of photometric redshift is so bad that it could increase contaminations. In Fig. 5, photometric redshifts are plotted against spectroscopic redshifts for confirmed galaxies. The standard deviation of $(z_{\rm spec} - z_{\rm phot})$ is 0.05 at $1.590 \leq z_{\rm spec} \leq 1.644$. Our photometric redshifts are fairly good for them. We selected only the objects that fall within a narrow redshift interval of $1.56 \leq z_{\rm phot} \leq 1.68$ since the $K$-band-selected galaxies can include contaminations at contiguous redshift unlike

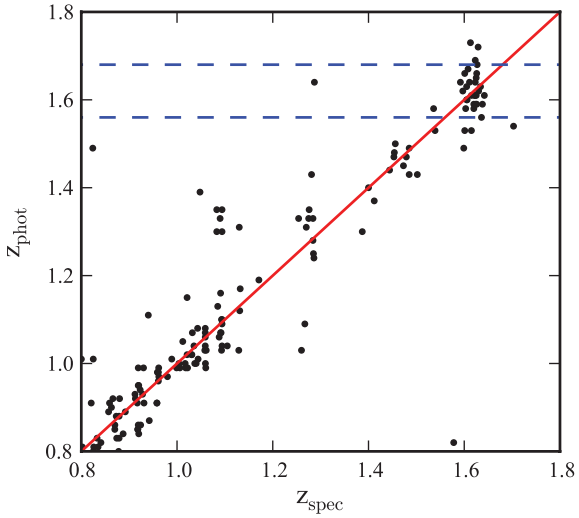


**Figure 5.** The spectroscopic redshift versus the photometric redshift for galaxies with $0.8 < z_{spec} < 1.8$. Red line is $z_{phot} = z_{spec}$. Blue dashed lines show the criterion of the photo-$z$ selected sample ($1.56 \leq z_{phot} \leq 1.68$).

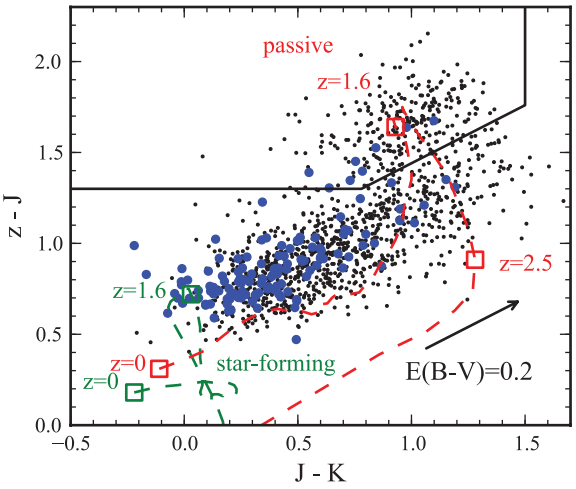


**Figure 6.** The $z - J$ versus $J - K$ colour–colour ($zJK$) diagram of the photo-$z$ selected galaxies (black dots). Blue circles show the [O II] emitter samples. Red dashed and green dashed lines show a model track of a passive galaxy and a star-forming galaxy, respectively (Kodama et al. 1998). The squares indicate the model colour at $z = 0$, 1.6 and 2.5. The arrow shows the dust reddening vector of $E(B - V) = 0.2$ (Calzetti et al. 2000). The solid lines show the adopted criteria to separate between quiescent galaxies and star-forming galaxies at $z = 1.6$.

the *NB*973 emitters. Such a stringent criterion of photometric redshift range is reasonable because our photometric redshifts are good enough to recover most of the spectroscopically confirmed cluster members. In fact, the photometric redshift distribution of the [O II] emitters shows a narrow concentration at $z \sim 1.6$ as shown in Fig. 3.

We have constructed a mass-limited sample with the stellar mass $M_{star} > 10^{10}$ M$_\odot$ on the basis of photometric redshifts. Stellar masses are estimated from the total $K$-band magnitudes, $K^{total}$, and $z - K$ colours, using the ratio between mass-to-luminosity ratio in $K$ band and $z - K$ colour of the population synthesis bulge–disk composite models (Kodama, Bell & Bower 1999) after it is scaled to the Salpeter initial mass function (IMF) for consistency. At $z = 1.6$, we used the following equations:

$$\log(M_{star}/10^{11}) = -0.4(K^{total} - 21.64), \quad (3)$$

$$\Delta \log M_{star} = 0.1 - 1.12 \exp[-0.82(z' - K)]. \quad (4)$$

The amount of contamination and that of completeness of the sample are estimated based on the spectroscopically confirmed galaxies. There are 32 galaxies with $M_{star} > 10^{10}$ M$_\odot$ which are located within $1.590 \leq z_{spec} \leq 1.644$. Since six spectroscopically confirmed cluster member galaxies do not fall within the photometric redshift range $1.56 \leq z_{phot} \leq 1.68$, the completeness can be estimated to be 81 per cent. We include them in our sample. Also, because our sample includes three objects at different spectroscopic redshift, from the cluster redshift, the contamination can be estimated to be 10 per cent. However, in order to accurately estimate them, we need to make more spectroscopic follow-up observations. 132 [O II] emitters with $M_{star} > 10^{10}$ M$_\odot$ satisfy our photometric redshift selection ($1.56 \leq z_{phot} \leq 1.68$). After excluding these [O II] emitters from our photo-$z$ selected sample, we constructed a non-emitter sample of 1174 galaxies.

It is known that cluster galaxies exhibit a conspicuous 'red sequence' on the colour–magnitude diagram which is mainly composed of passively evolving galaxies. The red sequence is well recognized even in distant clusters out to $z \sim 1$ (Kodama et al. 1998) and it persists at the bright end even in protoclusters at $z \sim 2$ (Kodama et al. 2007). The red sequence consists of not only passive galaxies, but also dusty star-forming galaxies, and we use a $zJK$ diagram to separate them in the same manner as in Williams et al. (2009). Fig. 6 shows the $zJK$ diagram for the photo-$z$ selected galaxies. Using the model colour tracks of Kodama et al. (1998) and the dust reddening vector (Calzetti et al. 2000), we defined the quiescent galaxies at $z = 1.6$ using three criteria: $z - J > 1.3$, $J - K < 1.6$ and $z - J > 0.64(J - K) + 0.8$. In total, 259 quiescent galaxies have been selected from photo-$z$ selected sample. On the other hand, there are a number of blue galaxies (915) in photo-$z$ selected sample. It is likely that either their [O II] emissions are too weak to be detected as the narrow-band excess or they are outside of the redshift range of the *NB*973 filter ($z < 1.590$ or $z > 1.644$). Since the contamination of the latter objects is probably large, we do not use those blue galaxies in our analyses. Three quiescent galaxies have been spectroscopically confirmed and a spectral fit of the brightest member yields an age of 1.8 Gyr with a mass of $3.8 \times 10^{11}$ M$_\odot$ in Salpeter IMF (Tanaka et al. 2010). Because most of the galaxies with spectroscopic redshift are line emitters, a follow-up spectroscopy is needed to confirm whether other quiescent galaxies are truly cluster members.

We thus constructed a combined sample of the photo-$z$ selected and mass-limited galaxies at $1.56 \leq z_{phot} \leq 1.68$, composed of 132 [O II] emitters and 259 quiescent galaxies. Table 1 gives a summary of our galaxy samples used in this paper.

**Table 1.** The numbers of our photo-$z$ selected samples at $1.56 \leq z_{phot} \leq 1.68$.

| Sample | Cluster | Field | Total |
|---|---|---|---|
| Star-forming [O II] emitters | 74 | 50 | 124 |
| Red [O II] emitters | 4 | 4 | 8 |
| Quiescent galaxies | 86 | 173 | 259 |
| Combined sample | 164 | 227 | 391 |

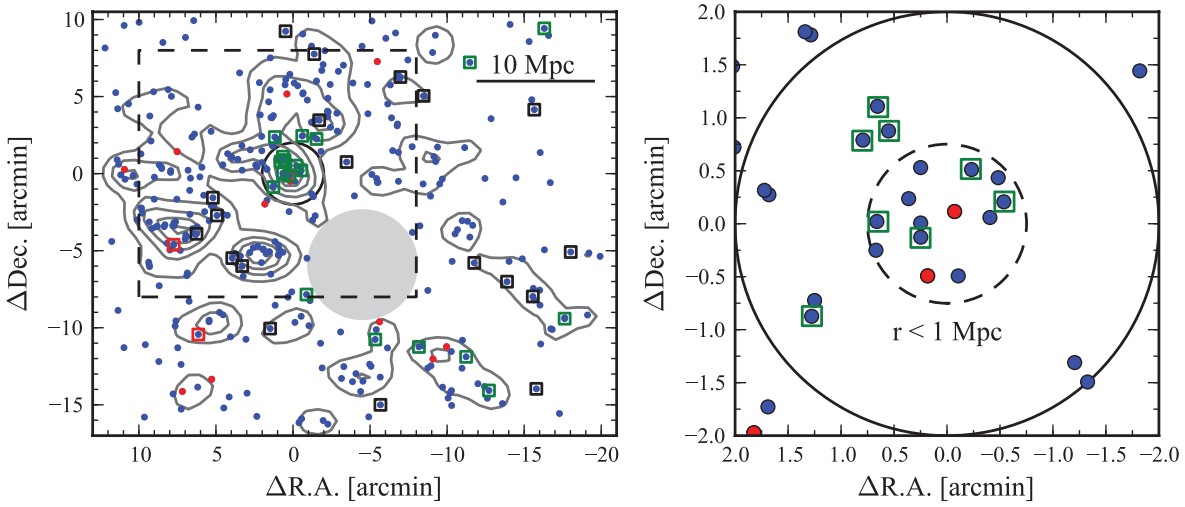


**Figure 7.** Left: the 2D distributions of 352 [O II] emitters. Blue and red filled circles show star-forming and red [O II] emitters, respectively. Squares indicate the spectroscopically confirmed objects with $1.590 \leq z_{\rm spec} < 1.620$ (black), $1.620 \leq z_{\rm spec} \leq 1.630$ (green) and $1.630 < z_{\rm spec} \leq 1.644$ (red). Contours denote the local number density of [O II] emitters. Outside of dash lines is the field region defined in Section 4.1. The grey filled circle is a masked region near a bright star. Right: close-up view of the cluster core ($r < 2$ arcmin). Dashed line circle shows the radius of $r = 1$ Mpc. Note that our *NB*973 filter can prove about ±47 Mpc (comoving) in the redshift direction.

## 4 RESULT

### 4.1 Spatial distribution

With the panoramic imaging of the $z = 1.62$ cluster with Suprime-Cam, we have revealed a gigantic structure surrounding the cluster traced by [O II] emitters for the first time, as shown in Fig. 7. The cluster appears to be embedded in a huge filament extending from north to east/south. In particular, there are two dense regions to the east/south and to the south of the cluster, respectively. Also, a filament of relatively dense region extends to the north. They all appear to be associated with the cluster core and constitute a huge structure of about 20 Mpc in comoving scale.

Many star-forming [O II] emitters are located within the projected radius of 1 Mpc in comoving scale from the cluster centre. This is in stark contrast to the nearby Universe where galaxies in dense environment tend to be inactive red galaxies and star-forming galaxies are preferentially located in lower density environments. We evaluated the overdensity of the [O II] emitters in the cluster core ($r < 1$ Mpc). The average number density of the [O II] emitters is 0.24 Mpc$^{-2}$ (352/1472) for the entire region of the survey (∼1472 Mpc$^2$). This value is roughly comparable to the number density (0.35 Mpc$^{-2}$) expected from the [O II] luminosity function at $z = 1.47$ in the general field (Ly et al. 2007) because the criterion of the equivalent width in our selection is more stringent than the one used in the previous studies. On the other hand, since 13 [O II] emitters exist in the cluster core (∼3.142 Mpc$^2$), the number density is 4.14 Mpc$^{-2}$, which is about 17 times larger than that in the entire region. The quiescent galaxies show the overdensity by a factor of 9. This clearly indicates that the star formation activity has not been ceased yet even in the core of the $z = 1.62$ cluster, and rather the integrated star formation activity in the unit volume is actually higher in the cluster core than in the lower density regions.

Note that our narrow-band filter is probing ∼94 Mpc (comoving) in the redshift direction, and the 2D overdensity may not be free from the projection effect. In order to robustly measure the overdensity, the spectroscopic redshifts would be required. In fact, it is found from the FMOS spectroscopy that the [O II] emitters in the east and the south clumps are located at somewhat different redshifts from the cluster centre (Fig. 7). This difference corresponds to 1000–2000 km s$^{-1}$ in the line-of-sight velocity or to 15–30 Mpc in the comoving distance. It is not clear at this stage whether these clumps are gravitationally bound, physically associated systems to the cluster. More intensive spectroscopic follow-up observations are needed to address this issue.

### 4.2 Density dependence

It is widely recognized that the star formation activity of a galaxy is strongly related to the local density of galaxies surrounding it. In the local Universe, the star-forming activity decreases with increasing local galaxy density (Gómez et al. 2003; Patel et al. 2009). This relation holds out to at least $z \sim 0.8$ (e.g. Kodama et al. 2001; Tanaka et al. 2005). At $z \sim 1$, it is suggested that SFR–density relation may, in part, be inverted relative to the local relation (Elbaz et al. 2007; Cooper et al. 2008). However, these studies do not include the very dense environment such as rich cluster cores. In the ClG J2018−0510 cluster at $z = 1.62$, Tran et al. (2010) reported that the relative fraction of star-forming galaxies increases with increasing local density based on the SFRs derived from the 24-μm fluxes and the SED fitting. Note that they used sample based on only photometric redshift. On the other hand, Quadri et al. (2012) claimed that the star formation–density relation holds out to at least $z \sim 1.8$, although they similarly selected sample on the basis of the photometric redshift. In the case of photo-$z$ selected sample, any results must be interpreted with caution due to a large contamination. Therefore, the reversal of SFR–density relation at $z > 1$ is very controversial at this stage.

Our panoramic narrow-band survey of the [O II] emitters enables us to investigate the environmental dependence over a much larger area, hence covering a much wider range in environment. Moreover, due to the great advantage of the narrow-band imaging survey combined with photometric redshifts, our [O II] emitters are more robust members of star-forming galaxies associated with the cluster even without spectroscopy because we just need to separate out [O II]

emitters at $z \sim 1.6$ among a few other possibilities of different redshifts (corresponding to other lines) based on photometric redshifts. In order to discuss the environmental effect, we define the local density within the circled area of a radius to the 5th nearest neighbour object ($\Sigma_{5\mathrm{th}}$), by using the combined sample of $z \sim 1.6$ galaxies (Section 3.3). And we calculated the fraction of each sample among the combined sample, i.e. $f = N_{\mathrm{each\ sample}}/N_{\mathrm{combined\ sample}}$ at each bin of the local density. However, due to the photometric redshift selection, contaminations would dominate the number density in the low-density regions. Therefore, we do not use sample in the field region and concentrated on the region within the dashed rectangle in Fig. 7, and trust only the range of local number density that is more than the field density ($\Sigma_{5\mathrm{th,combined}} > 1.5\,\mathrm{Mpc}^{-2}$). The quiescent galaxies' sample inevitably contains some foreground or background objects because the photometric redshift range that we adopted ($\Delta z_{\mathrm{phot}} = 0.12$) is larger than that of the [O II] emitters ($\Delta z_{\mathrm{NB}} = 0.054$). We tried to correct for this effect by multiplying $\Delta z_{\mathrm{NB}}/\Delta z_{\mathrm{phot}}$ to the number of quiescent galaxies, assuming conservatively that their redshift distribution is uniform. As shown in Fig. 8, the fraction of star-forming galaxies in the combined sample does not show a significant dependence on the local density at $z \sim 1.6$. It is consistent with a constant value (~60 per cent) across different environments within errors. Star-forming activity in the cluster core is very high in this cluster, and the well-established star formation–density relation in the local Universe no longer exists. Although a lot of massive quiescent galaxies do exist in the high-density environment such as the cluster core, the star formation activity has not been ceased yet. Rather the integrated SFR per unit volume is actually much higher in the cluster core due to its high overdensity of the emitters.

In order to quantitatively compare the properties of the individual [O II] emitters as a function of environment, we estimate stellar mass, SFR and SSFR (SSFR = SFR/$M_{\mathrm{star}}$) for the [O II] emitters. [O II] emission line is widely used as a good SFR indicator, but strongly depends on metallicity and dust extinction. [O II]–SFR relation is recently being calibrated by using lower redshift samples

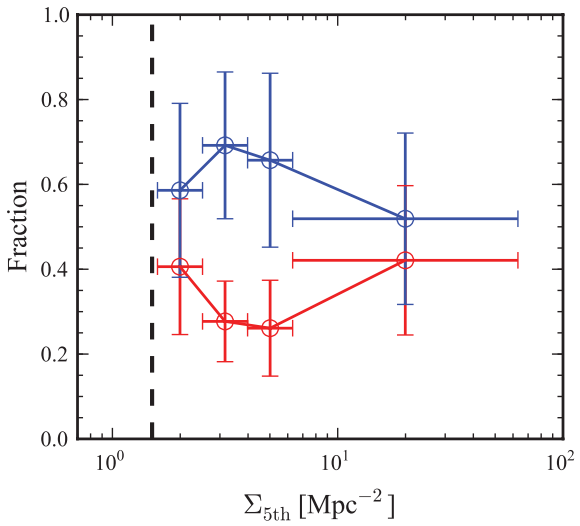


**Figure 8.** Relative fractions of [O II] emitters (blue circles) and quiescent galaxies (red circles) plotted as a function of local density. The local density is calculated from the combined samples of [O II] emitters and quiescent galaxies. Dashed line shows the number density in the field region (~1.5 Mpc$^{-2}$). In our analysis, we did not use the area below this density. Vertical and horizontal error bars indicate the Poissonian errors and the sizes of each bin, respectively.

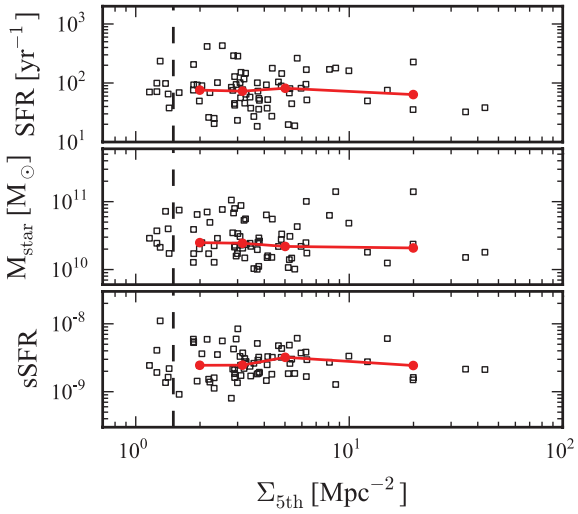


**Figure 9.** SFRs (top), stellar masses (middle) and SSFRs (bottom) for individual [O II] emitters, plotted against the local density. The local density is calculated from the combined samples of [O II] emitters and quiescent galaxies. Red circles show the median value in each density bin.

(Gilbank et al. 2010; Sobral et al. 2012). We used the [O II]–SFR calibration given by Sobral et al. (2012), which is described as a function of stellar mass. The results are shown in Fig. 9 as a function of local density. We do not find any significant environmental dependence in all of the individual quantities of the [O II] emitters. In fact, the median values of all the three quantities are almost constant with local density. Tadaki et al. (2011) claimed that the averaged star formation activity is rapidly declined from $z = 2.5$ to 0.8 in high-density regions such as clusters, while it is only gradually declined in the low-density regions. At some point at high redshifts, we may expect that the averaged SFR of galaxies in cluster cores should exceed that in the general field probably because galaxy formation processes (such as gas cooling and mergers) are accelerated in dense environments. The fact that we observe just a comparable level of star formation activity in the [O II] emitters irrespective of environment may suggest that, at $z = 1.62$, the [O II] emitters in the high-density regions are just in the transition phase from a starbursting mode to a quiescent mode as a result of environmental effect.

## 5 SUMMARY

We have conducted a narrow-band survey of [O II] emitters in and around the ClG J0218.3−0510 cluster at $z = 1.6$, using Suprime-Cam on Subaru. The observation with $z_R$ filter was newly carried out to measure the continuum at the same wavelength as the narrow-band filter (*NB*973). We combined these data with multi-broad-band data ($B, V, R, i', z', J, H, K$, 3.6, 4.5 μm) to create the *NB*973-detected and $K$-detected photometric catalogues. The photometric redshifts were determined with 11 bands including $z_R$ band. By comparing the spectroscopic members and our [O II] emitter sample, we estimated that the accuracy of our photometric redshifts is $\sigma_z = 0.05$ at $z = 1.6$. Our main results with these samples are summarized as follows.

(i) On the basis of narrow-band excesses and photometric redshifts, our survey provides a sample of 352 [O II] emitters over a 830 arcmin$^2$ area. Our very recent FMOS near-infrared spectro-

scopic observations have confirmed 31 [O II] emitters at $z \sim 1.6$ by the presence of H$\alpha$ or [O III] lines at the expected wavelengths. The [O II] emitters constitute a large-scale structure at $z = 1.62$ in which the ClG J0218.3−0510 cluster is embedded. Also, we find that many star-forming [O II] emitters are located even in the cluster core ($r < 1$ Mpc in the comoving scale) and in the surrounding clumps, and show a high overdensity by a factor of 17 compared to the entire region. This suggests that the integrated star formation activity per unit volume is activated in such regions.

(ii) The galaxies with $1.56 \leq z_{\rm phot} \leq 1.68$ show a clear bimodal distribution in the *zJK* diagram, namely quiescent and star-forming galaxies. We selected total of 259 quiescent galaxies on the basis of the population synthesis model and the extinction law by dust.

(iii) We calculated the local number density of galaxies in the photo-*z* selected and mass-limited sample to examine the environmental dependence of the star formation activity. We obtain a large fraction of [O II] emitters even in the cluster core, showing that the star-forming activity in the cluster core is elevated substantially compared to the local clusters where there are little star-forming galaxies in their cores. There is no longer an environmental dependence in the relative fraction of [O II] emitters in the combined sample, and the well-known SFR–density relation in the present-day Universe no longer exists within errors. Furthermore, the properties of the individual [O II] emitters, such as SFRs, stellar masses and SSFRs, do not depend on the local density, either. These results suggest that the [O II] emitters in the high-density regions are just in the transition phase from a starbursting mode to a quiescent mode due to some environmental effects and the SFRs in these systems may be rapidly declining.

Note that the results presented in this paper for the environmental effect of galaxies in and around a $z = 1.62$ cluster may not necessarily apply to all the clusters at the same epoch of the Universe, and the results may well depend on the degree of maturity of clusters even at the same redshift. For this reason, we require a systematic studies of distant clusters and general fields to construct a more general picture, and the MAHALO-Subaru project (Kodama et al., in preparation) will provide us more comprehensive views of galaxy evolution at its most active phase in the Universe.

## ACKNOWLEDGMENTS

This paper is based on data collected at Subaru Telescope, which is operated by the National Astronomical Observatory of Japan. We thank the Subaru Telescope staffs for their help in the observation. We also thank the anonymous referee for many useful comments, which improved the paper. TK acknowledges the financial support in part by a Grant-in-Aid for the Scientific Research (No. 21340045) by the Japanese Ministry of Education, Culture, Sports, Science and Technology. YK acknowledges the support from the Japan Society for the Promotion of Science (JSPS) through JSPS research fellowships for young scientists.

## REFERENCES

Baldwin J. A., Phillips M. M., Terlevich R., 1981, PASP, 93, 5
Bauer A. E., Grützbauch R., Jørgensen I., Varela J., Bergmann M., 2011, MNRAS, 411, 2009
Bertin E., Arnouts S., 1996, A&AS, 117, 393
Brammer G. B., van Dokkum P. G., Coppi P., 2008, ApJ, 686, 1503
Brodwin M. et al., 2011, ApJ, 732, 33
Bunker A. J., Warren S. J., Hewett P. C., Clements D. L., 1995, MNRAS, 273, 513
Calzetti D., Armus L., Bohlin R. C., Kinney A. L., Koornneef J., Storchi-Bergmann T., 2000, ApJ, 533, 682
Cooper M. C. et al., 2008, MNRAS, 383, 1058
Dressler A., 1980, ApJ, 236, 351
Dressler A. et al., 1997, ApJ, 490, 577
Elbaz D. et al., 2007, A&A, 468, 33
Fassbender R. et al., 2011, A&A, 527, L10
Furusawa H. et al., 2008, ApJS, 176, 1
Gilbank D. G., Baldry I. K., Balogh M. L., Glazebrook K., Bower R. G., 2010, MNRAS, 405, 2594
Gobat R. et al., 2011, A&A, 526, A133
Gómez P. L. et al., 2003, ApJ, 584, 210
Hayashi M., Kodama T., Koyama Y., Tanaka I., Shimasaku K., Okamura S., 2010, MNRAS, 402, 1980
Hayashi M., Kodama T., Koyama Y., Tadaki K. I., Tanaka I., 2011, MNRAS, 415, 2670
Henry J. P. et al., 2010, ApJ, 725, 615
Hewett P. C., Warren S. J., Leggett S. K., Hodgkin S. T., 2006, MNRAS, 367, 454
Hodgkin S. T., Irwin M. J., Hewett P. C., Warren S. J., 2009, MNRAS, 394, 675
Iwamuro F. et al., 2012, PASJ, in press
Kauffmann G. et al., 2003, MNRAS, 346, 1055
Kauffmann G., White S. D. M., Heckman T. M., Ménard B., Brinchmann J., Charlot S., Tremonti C., Brinkmann J., 2004, MNRAS, 353, 713
Kennicutt R. C., Jr, 1998, ARA&A, 36, 189
Kimura M. et al., 2010, PASJ, 62, 1135
Kodama T., Arimoto N., Barger A. J., Arag'on-Salamanca A., 1998, A&A, 334, 99
Kodama T., Bell E. F., Bower R. G., 1999, MNRAS, 302, 152
Kodama T., Smail I., Nakata F., Okamura S., Bower R. G., 2001, ApJ, 562, L9
Kodama T., Tanaka I., Kajisawa M., Kurk J., Venemans B., De Breuck C., Vernet J., Lidman C., 2007, MNRAS, 377, 1717
Koyama Y., Kodama T., Shimasaku K., Hayashi M., Okamura S., Tanaka I., Tokoku C., 2010, MNRAS, 403, 1611
Koyama Y., Kodama T., Nakata F., Shimasaku K., Okamura S., 2011, ApJ, 734, 66
Kron R. G., 1980, ApJS, 43, 305
Lawrence A. et al., 2007, MNRAS, 379, 1599
Lemaux B. C., Lubin L. M., Shapley A., Kocevski D., Gal R. R., Squires G. K., 2010, ApJ, 716, 970
Lewis I. et al., 2002, MNRAS, 334, 673
Ly C. et al., 2007, ApJ, 657, 738
Miyazaki S. et al., 2002, PASJ, 54, 833
Muzzin A. et al., 2012, ApJ, 746, 188
Ota K. et al., 2010, ApJ, 722, 803
Ouchi M. et al., 2004, ApJ, 611, 660
Papovich C. et al., 2010, ApJ, 716, 1503
Patel S. G., Holden B. P., Kelson D. D., Illingworth G. D., Franx M., 2009, ApJ, 705, L67
Postman M., Geller M. J., 1984, ApJ, 281, 95
Quadri R. F., Williams R. J., Franx M., Hildebrandt H., 2012, ApJ, 744, 88
Simpson C. et al., 2012, MNRAS, 421, 3060
Skrutskie M. F. et al., 2006, AJ, 131, 1163
Smail I., Sharp R., Swinbank A. M., Akiyama M., Ueda Y., Foucaud S., Almaini O., Croom S., 2008, MNRAS, 389, 407
Sobral D. et al., 2009, MNRAS, 398, 75
Sobral D., Best P. N., Smail I., Geach J. E., Cirasuolo M., Garn T., Dalton G. B., 2011, MNRAS, 411, 675
Sobral D., Best P. N., Matsuda Y., Smail I., Geach J. E., Cirasuolo M., 2012, MNRAS, 420, 1926
Tadaki K. I., Kodama T., Koyama Y., Hayashi M., Tanaka I., Tokoku C., 2011, PASJ, 63, 437

Tanaka M., Kodama T., Arimoto N., Okamura S., Umetsu K., Shimasaku K., Tanaka I., Yamada T., 2005, MNRAS, 362, 268
Tanaka M., Finoguenov A., Ueda Y., 2010, ApJ, 716, L152
Tanaka M. et al., 2012, PASJ, 64, 22
Tran K. et al., 2010, ApJ, 719, L126
Ueda Y. et al., 2008, ApJS, 179, 124
Whitmore B. C., Gilmore D. M., Jones C., 1993, ApJ, 407, 489
Williams R. J., Quadri R. F., Franx M., van Dokkum P., Labbé I., 2009, ApJ, 691, 1879
Yagi M., Kashikawa N., Sekiguchi M., Doi M., Yasuda N., Shimasaku K., Okamura S., 2002, AJ, 123, 66
Yan R., Newman J. A., Faber S. M., Konidaris N., Koo D., Davis M., 2006, ApJ, 648, 281

This paper has been typeset from a TEX/LATEX file prepared by the author.